Modeling Highly Efficient Homojunction Perovskite Solar Cells With Graphene-TiO_2 Nanocomposite as the Electron Transport Layer

Nabarun Saha, Giuseppe Brunetti, Mario N. Armenise, Aldo Di Carlo, and Caterina Ciminelli, *Senior Member, IEEE*

***Abstract*—Perovskite-based solar cells have observed tremendous growth in the last decade aiming at developing renewable energy sources. The enhancement of the power conversion efficiency (PCE), sustainability, and easing of the fabrication are the main driving forces of the ongoing research activity. In this context, graphene is particularly promising since it not only provides better charge collection but also helps to improve the sustainability and low-temperature fabrication of the perovskite cell. Here, a homojunction $MaPbI_3$ perovskite solar cell with graphene-TiO_2 nano-composite as the electron transport layer (ETL) has been numerically investigated. The effect of doping concentration on the p and n-doped section in the homojunction-$MaPbI_3$ has been studied, showing that 10^{17} and 10^{16} cm^{-3} doping on the p and n section of $MaPbI_3$, respectively, provide the best band alignment with the ETL layer. The optimum thickness ratio of two doped sections (p:n) is found to be 60:40 in %. Moreover, the presence of graphene in the TiO_2 layer improves PCE thanks to enhanced fill factor and saturated current density. A combined effect of all these results in a PCE of 22.71% with a 100 nm thick ETL layer having an optimum graphene concentration of around 1%.**

***Index Terms*—Electron transport layer, graphene, nanocomposite, perovskite solar cell.**

I. Introduction

With the ever-growing population, the demand for sustainable energy sources is also growing. To meet this demand and to find out an alternative to pollutant energy sources like fossil fuels, researchers are in a continuous quest for cost-effective, eco-friendly energy sources. In this context, solar cells, which convert solar energy into electrical energy through the photovoltaic effect, have found particular interest over the years. Organic-inorganic-based metal halide perovskite solar cells [1], [2] have seen astonishing growth since their invention in 2009 [3] due to various advantages like direct band-gap, high absorption, high carrier mobility, cost-effectiveness, ease of fabrication, smaller exciton binding energy, useful for domestic and industrial power grids as well as space power supply [4].

In a typical perovskite solar cell, the absorbing layer of perovskite is placed in between two layers called the electron transport layer (ETL) and hole transport layer (HTL) to establish an efficient charge separation. However, the recombination of the photo-generated carriers taking place in various defects lying within the perovskite layer, ETL/HTL layer, or at the interfaces hinders the charge transport and collection. Therefore, to improve charge separation, transportation, and collection, different strategies have been reported in the last years [5], [6], [7], [8], [9]. One such attempt is to form a p-n homojunction in the absorbing layer of the perovskite. The in-build electric field generating at the p-n homojunction helps to improve the separation and the oriented transportation of the photo-generated carriers with a suppression of the recombination inside the absorbing layer. This, subsequently, leads to an improvement in power conversion efficiency. Cui et al. [9] fabricated a p-n homojunction-based perovskite solar cell that provides a PCE exceeding 21.3%. They have shown that by controlling the precursor ratio of PbI_2 and MaI, a p-n homojunction can be formed easily in the $MaPbI_3$. Following this, various attempts have been made by researchers to improve efficiency as well as stability using the homo-junction architecture [10], [11], [12]. For example, Maram et al. [10] numerically reported an efficiency 16.5% with homojunction perovskite in inverted configuration. Furthermore, Yousuf et al. [12] estimated a PCE of 28.2% with graded absorber layer in the homojunction configuration. But experimentally it is quite difficult to achieve such graded doping in the perovskite layer. It is to note that formation of homojunction itself provides oriented transportation of the photo-generated charge carriers, therefore, potential of ETL and HTL-free perovskite structure has also been investigated by different research groups [13], [14]. For example, Da et al. have reported a PCE of 26.3% by omitting the charge transport layers. However, the poor mismatch between the energy levels with the charge-collecting layers like metal and fluorine-doped tin oxide (FTO) in addition to recombination

Manuscript received 6 April 2023; revised 18 May 2023; accepted 20 June 2023. Date of publication 10 July 2023; date of current version 6 September 2023. This work was supported by the Ministry of Research and University through the Projects ARS01_01215 New Satellites Generation Components and ARS01_00141 Close to the Earth. *(Corresponding author: Caterina Ciminelli.)*

Nabarun Saha, Giuseppe Brunetti, Mario N. Armenise, and Caterina Ciminelli are with the Optoelectronics Laboratory, Politecnico di Bari, 70125 Bari, Italy (e-mail: nabarun.saha@poliba.it; giuseppe.brunetti@poliba.it; marionicola.armenise@poliba.it; caterina.ciminelli@poliba.it).

Aldo Di Carlo is with the Centre for Hybrid and Organic Solar Energy, Department of Electronic Engineering, University of Rome Tor Vergata, 00133 Rome, Italy, and also with the Institute for Structure of Matter, National Research Council, 00133 Rome, Italy (e-mail: aldo.dicarlo@uniroma2.it).

Color versions of one or more figures in this article are available at https://doi.org/10.1109/JPHOTOV.2023.3289574.

Digital Object Identifier 10.1109/JPHOTOV.2023.3289574

at the perovskite/charge-collecting layer interface hinders the practical realization of such structures. This effect highlights the importance of layers like ETL and HTL even in homojunction perovskites configurations. Therefore, it is important to improve the quality of such layers, which not only provides better charge collection but also eases the fabrication, improves stability, and provides relaxation in their thicknesses. Recently, it has been observed that the use of graphene or related two-dimensional (2-D) material can improve charge collection/injection of the transport layers, which enhances the power conversion efficiency [15], [16] as well as the capability of providing a long time of stability [17]. It is noted that graphene has several advantageous properties like high conductivity and high charge mobility, which improves charge carrier collection. However, the use of graphene nanolayer as a transport layer also causes large-scale recombination. Therefore, it is useful to use graphene as a doped element in the transport layer [18]. For example, Wang et al. [19] reported that utilizing graphene TiO_2 nano-composite as the ETL layer it is possible to significantly increase the PCE and reported an efficiency of 15.6% with conventional heterojunction perovskite structure. Furthermore, graphene nanoflakes in the TiO_2 layer not only improve the charge collection but also help to fabricate the entire structure at a temperature lower than 150 °C. Another low-temperature perovskite solar cell is reported in [20] with graphene in a compact and mesoporous TiO_2 layer showing an efficiency of 15.81%. In another approach with graphene-TiO_2 nanocomposite as the ETL layer, Belchi et al. [21] reported an efficiency of 15.3% but also with the heterojunction-based perovskite. So far to our knowledge, there is no report of graphene-TiO_2-assisted ETL layer with p-n homojunction perovskite architectures.

In this article, we report and numerically investigated a homojunction $MaPbI_3$-based perovskite solar cell with graphene-TiO_2 (gr-TiO_2) nanocomposite as the ETL layer. The homojunction perovskite layer and graphene in the TiO_2 ETL layer, respectively, provide efficient charge separation inside the absorbing layer due to built-in potential across p-n junction and efficient charge collection due to the high mobility of graphene. As a result, the combination of homojunction perovskite layer and gr-TiO_2 ETL produces a PCE of 22.71% with around 1% graphene concentration for a 100-nm thick ETL layer. The rest of this article is organized as follows. In Section II, we have discussed the basic structure and its working principle and modeling. The analysis has been carried out with the well-known and accurate solar cell capacitance simulator-one-dimensional (SCAPS-1D) simulation tool. In Section III, the effect of band alignment on the proposed structure has been investigated with different doping concentrations in the $MaPbI_3$ section along with the relative thickness of the two doped sections. Next, the effect of graphene concentration has been reported along with the impact of the defect densities in different layers and interfaces on the device performance. Overall, the proposed perovskite solar cell shows an excellent power conversion efficiency due to the combined effect of homojunction architecture and the presence of graphene nano-flakes in the ETL layer, which can further provide stability and ease the fabrication at lower temperatures.

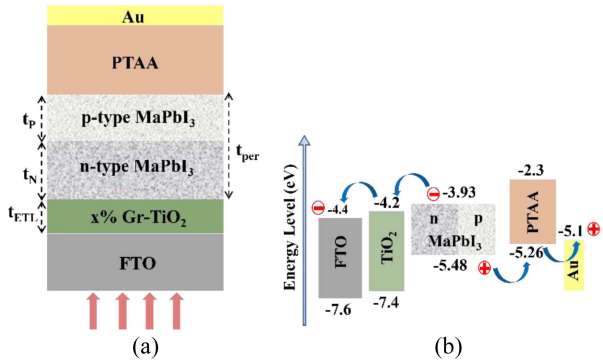

Fig. 1. (a) Stack diagram of the proposed perovskite cell and (b) layers energy band diagram explaining the charge transport phenomenon. The values are taken from [25] for FTO, [19] for TiO_2, [26] for $MaPbI_3$, and [27] for PTAA.

II. Proposed Structure and Modeling

The stack configuration of the proposed perovskite solar cell is shown in Fig. 1(a). It consists of graphene-doped TiO_2 (titanium dioxide) nano-composite as the ETL and poly[bis(4-phenyl)(24,6-trimethylphenyl)amine (PTAA) as the HTL. A metallic layer of gold (Au) and a transparent layer of FTO are used as the back and front contact, respectively. The perovskite absorption layer consists of $MaPbI_3$ in p-n homojunction configuration. The p-type $MaPbI_3$ can be realized by excess MA^+ or deficiency of Pb^{2+} whereas n-type can be accomplished with excess Pb^{2+} or the deficiency of Ma^+ or I^- [9]. Fig. 1(b) explains the working principle of the solar cell structure with the help of the energy band diagram. The light absorbed in the perovskite layer generates current flow on the structure with electrons and holes collected and transported through the ETL and HTL layer, respectively. The build-in potential in the p-n homojunction configuration facilitates the charge separation and, thus, helps to increase the efficiency. The graphene in the TiO_2 layer increases the mobility of the ETL layer and subsequently improves the charge collection. The thickness of the p-n homojunction layer should be higher than the depletion region formed at the interface of two doped sections in $MaPbI_3$, which can be calculated following the equation $t_{dep} = \sqrt{2\varepsilon_0\varepsilon_r V_{bi}/qN_{A/D}}$ where V_{bi} is the built-in voltage taken to be 1 volt, q is the electron charge, ε_r is the relative dielectric constant of the $MaPbI_3$ taken to be 25 [22], [23]. In our analysis, the lowest doping concentration is considered to be 10^{16}, which provides a depletion region's thickness to be $\sim$ 500 nm. Following this, the thickness of the $MaPbI_3$ (t_{per}) is chosen to be slightly higher, 540 nm [9], [23]. The thickness of the FTO and PTAA is considered to be 50 nm and 200 nm, respectively. The thickness of the graphene-doped TiO_2 layer and the relative thickness of the perovskite layer has been varied to study their effect on the performance of the proposed structure. The numerical analysis has been performed with the simulation tool SCAPS-1d, version 3.3.10 [24]. It basically solves three well-known equations: the Poisson equation and the continuity equations of electrons and holes

$$\frac{\partial^2\varphi}{\partial x^2} = -\frac{q}{\varepsilon_r}\left[p(x) - n(x) + N_D^+(x) - N_A^+(x) \pm N_t(x)\right] \quad (1)$$

TABLE I
DIFFERENT PARAMETERS USED TO SIMULATE THE PROPOSED STRUCTURE IN SCAPS-1D

Parameters	FTO [25]	TiO_2	5%gr+TiO_2	10%gr+TiO_2	n-type-$MaPbI_3$	p-type-$MaPbI_3$	PTAA [27]
χ (eV)	4.4	4.2 [19]	4.24 [26]	4.28 [26]	3.93 [23, 26]	3.93 [23, 26]	2.3
E_g (eV)	3.2	3.2 [19]	3.1 [26]	2.7 [26]	1.55 [14, 26]	1.55 [26]	2.96
ε_r	9	9 [26]	7.3 [26]	7.5 [26]	25 [9]	25 [9]	9
N_c (cm^{-3})	2.2×10^{18}	1×10^{21} [23]	1×10^{21} [23]	1×10^{21} [23]	2×10^{18} [19]	2×10^{18} [23]	2×10^{21}
N_v (cm^{-3})	1.8×10^{19}	2×10^{21} [23]	2×10^{21} [23]	2×10^{21} [23]	2×10^{18} [19]	2×10^{18} [23]	2×10^{21}
N_A (cm^{-3})	--	--	--	--	--	variable	1×10^{18}
N_D (cm^{-3})	1×10^{18}	5×10^{19} [23]	5×10^{19} [23]	5×10^{19} [23]	variable	--	--
μ_n/μ_p (cm^2/Vs)	2/1	0.02/0.2 [26]	12/12 [26]	125/125 [26]	10/10 [23]	10/10 [23]	1/40
τ_n/τ_p (ns)	--	5/2 [26]	2/2 [26]	1/1 [26]	20/20 [23]	20/20 [23]	--

$$\frac{\partial J_n}{\partial x} + G_n - R_n = 0 \tag{2}$$

$$-\frac{\partial J_p}{\partial x} + G_p - R_p = 0. \tag{3}$$

In the abovementioned equations, p and n are the free hole and electron concentration, N_D^+ and N_A^+ represent ionized donor and acceptor concentrations, N_t is the defect/trap density, G_n and G_p are the generation rates of electrons and holes, and R_n and R_p are the recombination rates of electrons and holes. The SCAPS-1D numerically solve the 1-D Poisson (1) to find out the electric filed distribution due to the space charge density at the p-n junctions. The continuity (2) and (3) with J_n and J_p being the electron and hole current density provides the variation of current density along the device thickness following the generation and recombination profile, which is shown in the following section. In order to solve these equations in SCAPS-1D model, the experimentally reported values of important parameters for the different layers in the proposed structure are added in the SCAPS-1-D, as shown in Table I [9], [19], [23], [25], [26], [27]. The doping concentration of the p-type and n-type sections in $MaPbI_3$ is varied between 10^{16} and 10^{17} cm^{-3}. As reported in [23], 10^{16} cm^{-3} is found to be the minimum doping concentration to form the p-n homojunction in $MaPbI_3$. The four most important parameters deciding the efficiency are open circuit voltage V_{oc}, saturation current density J_{sc}, fill factor FF and PCE denoted by η. The simulation has been carried out in the presence of in-built SCAPS-1d AM 1.5 G solar spectrum with 1000 W/m^2 solar density. The thermal velocity of the electron and holes are taken to be 10^7 cm/s. For the perovskite layer, the wavelength-dependent imaginary part of the dielectric constant has been used to calculate the absorption spectrum [28] whereas for other layers the SCAPS-1D absorption model has been used. In order to make a more accurate prediction of the proposed solar cell performance, a neutral defect density of 10^{14} cm^{-2} is considered at the two interfaces PTAA/p-type $MaPbI_3$ and n-type $MaPbI_3$/gr-TiO_2 with distinctive energy of 0.1 eV [29]. In order to match the reported time constant (τ_n/τ_p) of Shockley–Read–Hall (SRH) recombination for electrons/holes, the defect density of each layer has been adjusted properly in the SCAPS model. We have neglected the Auger recombination due to its extremely low recombination coefficient (2.3×10^{-29} cm^6/s) for the perovskite [30]. The radiation recombination coefficient is considered to be 1.1×10^{-10} cm^3/s [30].

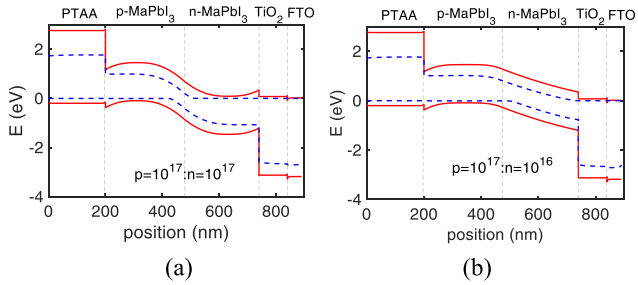

Fig. 2. Energy band diagram for two different doping concentrations of n (p) side of $MaPbI_3$ (a) 10^{17} cm^{-3} (10^{17} cm^{-3}) and (b) 10^{16} cm^{-3} (10^{17} cm^{-3}).

III. RESULTS AND DISCUSSIONS

A. Analysis of Band Alignment

The performance of solar cells largely depends on the band alignment of the perovskite layer with the ETL and HTL layers. Furthermore, it has been observed that the doping concentration of two sides of the $MaPbI_3$ in addition to their relative thickness has an important role to play in deciding the band alignment and thus the efficiency. In view of that, first, a detailed band alignment study has been performed with gr-TiO_2 nano-composite as the ETL layer. Initially, the graphene concentration is taken to be 0% to investigate the effect of doping concentration and relative thickness of the two doped sections of $MaPbI_3$. Two different sets of doping concentrations have been considered. The corresponding band diagram has been shown in Fig. 2. The thickness of the two doped sides of $MaPbI_3$ is taken to be 270 nm each whereas the thickness of the TiO_2 is taken to be 100 nm. As can be seen from Fig. 2(a) when the doping concentration on both sides is 10^{17} cm^{-3}, a spike has been formed at the n-type $MaPbI_3/TiO_2$ interface, impeding the flow of electrons. As a result, the recombination rate also increases at this interface. The generation and recombination profiles for the two sets of doping concentrations are reported in Fig. 3(a) and (b), respectively. Fig. 3(a) depicts that the carrier generation is taking

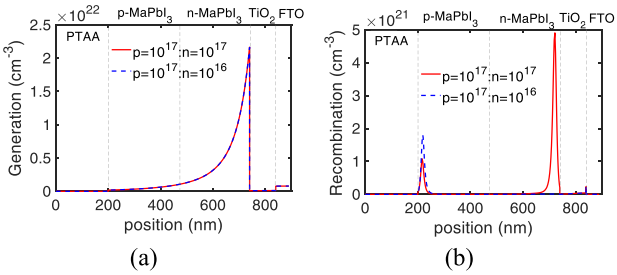

Fig. 3. (a) Generation profile and (b) recombination profile for two different sets of doping concentrations.

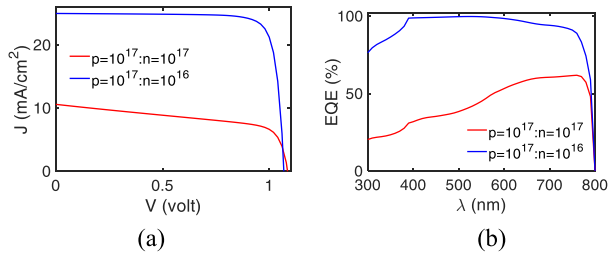

Fig. 4. (a) J-V characteristics and (b) EQE for two sets of doping concentrations.

place in the perovskite layer with a maximum at the n-type $MaPbI_3/TiO_2$ interface and exponentially decaying towards the p-type $MaPbI_3$/PTAA interface. The recombination profile is showing a large spike at the n-type $MaPbI_3/TiO_2$ interface for the equal doping concentration of 10^{17} cm^{-3}, which can be attributed to the spike in the energy band diagram, creating a potential barrier against the flow of electrons. In order to avoid this recombination, the doping concentration on the n-type $MaPbI_3$ has been reduced to 10^{16} cm^{-3}. This help to decrease the slope at the p-n homojunction as can be seen from the two energy band diagrams. As a result, the energy band shows a better alignment and removes the spike at the n-type $MaPbI_3/TiO_2$ interface. Fig. 3(b) shows that the spike in the recombination profile at the n-type $MaPbI_3/TiO_2$ interface is absent for the doping concentration of 10^{16} cm^{-3}, therefore a better efficiency can be expected with a doping concentration of 10^{16} cm^{-3} in the n-doped side. It is to note that the recombination rate also has a spike near the p-type $MaPbI_3$/PTAA interface, but it is much smaller than the n-type $MaPbI_3/TiO_2$ interface.

In order to investigate the effect of band alignment on the output characteristics, the J-V graph is plotted in Fig. 4(a) for two different sets of doping concentrations as mentioned previously. The figure clearly shows that when the doping concentration of the n-doped section of $MaPbI_3$ is reduced from 10^{17} cm^{-3} to 10^{16} cm^{-3}, J_{sc} increases significantly owing to the absence of the potential barrier, as discussed previously. The J_{sc} is found to be increased from 10.59 mA/cm^2 to 24.98 mA/cm^2 when the doping concentration of the n-side reduced from 10^{17} cm^{-3} to 10^{16} cm^{-3}, keeping the doping density on the p-side of $MaPbI_3$ fixed at 10^{17} cm^{-3}. The corresponding solar cell efficiency has been increased from 6.86% to 22.38%, thanks to the better band alignment. In order to establish further that the proposed structure has better charge collection capacity with n-side doping

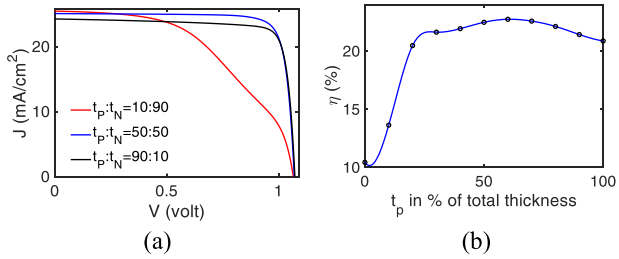

Fig. 5. (a) J-V graphs for three different thickness ratios of two doped sections of $MaPbI_3$ with a fixed total thickness of 540 nm. (b) Variation of PCE (η) with the different thickness of the p-doped section in % of total thickness 540 nm.

concentration of 10^{16} cm^{-3}, the external quantum efficiency (EQE) is calculated which basically represents the ratio between the number of charge carriers collected and the number of incident photon. Fig. 4(b) shows the EQE as a function of wavelength. Due to the absence of a potential barrier, a better charge collection is possible from the solar cell for the n-side doping concentration of 10^{16} cm^{-3}. As a result, a significant enhancement in EQE has been achieved with a doping concentration of 10^{16} cm^{-3} as evident from the figure. The certain change in EQE below 400 nm is due to the lower absorption coefficient of the $MaPbI_3$ absorbing layer [28].

Henceforward, in our analysis, the doping concentration of the p-doped and n-doped sections of the $MaPbI_3$ is considered to be 10^{17} cm^{-3} and 10^{16} cm^{-3}, respectively. Next, we studied the J-V characteristics to find out the optimum thickness ratio of the two doped sections. In Fig. 5(a), three J-V graphs are plotted for three different thickness ratios (t_P:t_N). Here, we like to mention that the relative thickness of the two sections is modified keeping the entire perovskite layer's thickness fixed at 540 nm, which has been represented by thickness ratio t_P:t_N. For example, the thickness ratio 10:90, 50:50, and 90:10 in percentage gives us a relative thickness of 54 nm (486 nm), 270 nm (270 nm), and 486 nm (54 nm) for the p-doped (n-doped) section. For a thickness ratio of 10:90, the J-V characteristics show a double diode-like behavior. Due to the low FF of 50.76%, the efficiency is very low 13.58%. As the thickness of the p-doped section increases, the double diode-like behavior disappears, resulting in better performance. This is visible in two other J-V graphs having a thickness ratio 50:50 and 90:10. However, the J_{sc} is found to be decreasing at the higher thickness of the p-section. Therefore, to find out the optimum thickness ratio, Fig. 5(b) illustrates the variation of efficiency with the relative thickness of the p-doped section in %. The efficiency is found to be increasing as the thickness of the p-doped section increases and starts to decrease after a certain thickness ratio of the p-side. At a lower thickness of the p-side, the efficiency is low, which can be attributed to the low FF owing to double diode-like behavior. When the thickness of the p-side is higher, the saturated current density is found to be decreasing. As a result, after a certain thickness, the efficiency decreases. The efficiency reaches a maximum value at 60% thickness of the p-doped section. Therefore, in our further calculations, the thickness ratio of the p and n-doped section is considered to be 60:40, resulting in a thickness of 324 nm and 216 nm, respectively.

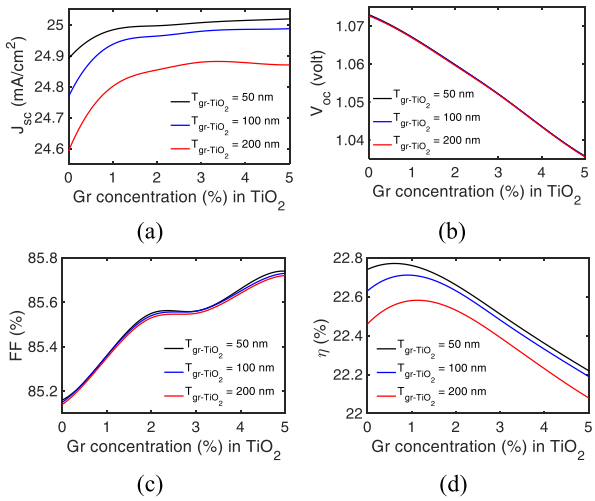

Fig. 6. Variation of (a) saturated current density, (b) open circuit voltage, (c) fill factor, and (d) power conversion efficiency as a function of graphene (Gr) concentration for three different thicknesses of the gr-TiO_2 nanocomposite ETL layer.

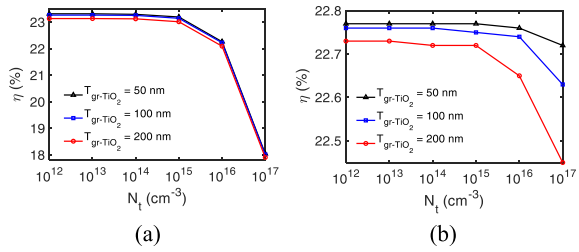

Fig. 7. Variation of proposed structure's power conversion efficiency with defect density in (a) $MaPbI_3$ and (b) gr-TiO_2.

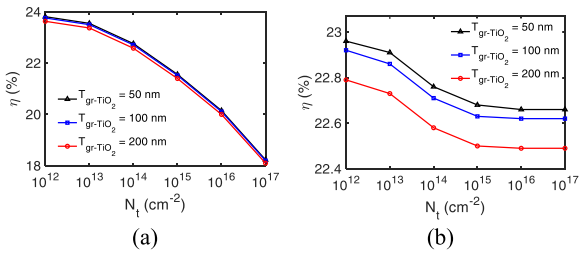

Fig. 8. Variation of PCE with the defect density at (a) n-$MaPbI_3$/gr-TiO_2 interface and (b) PTAA/p-$MaPbI_3$ interface.

B. Effect of Graphene in the ETL

In order to investigate the effect of graphene in the ETL layer and to find out the optimum doping concentration of graphene in the gr-TiO_2 nano-composite, available data (see Table I) is spline fitted for different parameters like band-gap (E_g), electron affinity (χ), dielectric constant (ε_r), mobility (μ_n/μ_p), and SRH recombination time (τ_n/τ_p). For example, the spline-fitted values for the aforementioned parameters are found to be 3.22, 4.21, 8.4, 2.56, and 4.19, respectively, at 1% of graphene concentration in gr-TiO_2 nano-composite. In the fitting, the piecewise cubic spline fitting is used in the MATLAB curve fitting having a smoothing parameter to be 1 for each data set. The four important parameters J_{sc}, FF, V_{oc}, and PCE have been plotted as a function of graphene concentration for three different thicknesses of the gr-TiO_2 nanocomposite-based ETL layer in Fig. 6. The saturated current density J_{sc} increases with the increment in the graphene concentration in the nano-composite of gr-TiO_2, as visible in Fig. 6(a). This can be attributed to the enhancement of mobility in the ETL layer with the rise of graphene concentration. In addition, some carrier generation in the ETL layer also contributes to the increment in J_{sc}. However, with the increase in graphene concentration, the defects in the gr-TiO_2 layer also increase, reducing the SRH time constant (τ_n/τ_p). Due to this combined effect, after a certain graphene concentration, J_{sc} saturates. The open circuit voltage V_{oc} is found to be decreasing with the increase in graphene concentration [see Fig. 6(b)] due to the conduction band offset (CBO) between the perovskite and gr-TiO_2 layer. As the graphene concentration increases, the electron affinity is found to be increasing. This results in higher CBO, lowering the value of V_{oc} [31], [32]. Another important parameter FF shows an increasing behavior with the graphene concentration as visible in Fig. 6(c). Graphene in the TiO_2 improves the charge collection efficiency of the ETL layer, enhancing the FF. Due to the combined effect of all these parameters the PCE of the proposed structure is found to be increasing with the rise in the graphene concentration as evident from Fig. 6(d). For each thickness value of the ETL layer, at a certain point, the PCE reaches the maximum and starts to decrease. For example, at 100 nm thick gr-TiO_2 layer, the optimum graphene concentration is found to be around 1%, in good agreement with experimentally reported results in heterojunction perovskite solar cell with gr-TiO_2 nanocomposite as the ETL layer [19]. Fig. 6(d) also shows that with the increase in gr-TiO_2 layer's thickness, the maximum efficiency point moves to the higher doping concentration and the maximum efficiency value also reduces. It is to note that the effect of the gr-TiO_2 thickness is more prominent on the J_{sc}. The higher thickness of the gr-TiO_2 layer increases the propagation length of the charge carriers. Therefore, greater possibility of recombination decreases the number of charge carriers, reducing the value of J_{sc} and, thus, efficiency.

The defect density plays a crucial role in deciding the PCE of the perovskite solar cells as it reduces the SRH recombination time. In view of that, the effect of defect densities in the perovskite layer and gr-TiO_2 layer in addition to two interfaces p-type $MaPbI_3$/PTAA and n-type $MaPbI_3$/gr-TiO_2 have been investigated by taking graphene concentration equal to 1%. Fig. 7(a) and (b) illustrates the variation of PCE with the defect density in the $MaPbI_3$ and gr-TiO_2, respectively. The PCE is found to be almost constant up to a defect density of 10^{15} cm^{-3} and then starts reducing, which is more prominent after a defect density of 10^{16} cm^{-3}. The defect density in the gr-TiO_2 layer has a much lower impact on the PCE of the structure as evident from Fig. 7(b). After a defect density of 10^{15} cm^{-3}, the PCE reduces rapidly for a higher thickness of the gr-TiO_2 layer. This is expected since thicker gr-TiO_2 contains more defect centers thus a greater possibility of recombination. Fig. 8(a) and (b), respectively, illustrates the variation of PCE with the interface defect density at the n-$MaPbI_3$/gr-TiO_2 and PTAA/p-$MaPbI_3$ interface. It is observed that the effect of interface defect density is more prominent at the n-$MaPbI_3$/gr-TiO_2 interface. The efficiency is found to be decreasing almost linearly with an increase in interface defect density. The PCE shows a much more stable performance with respect to the defect density variation at the PTAA/p-$MaPbI_3$ interface, as visible in Fig. 8(b).

IV. Conclusion

We report a novel homojunction $MaPbI_3$-based perovskite solar cell with graphene-TiO_2 nanocomposite as the ETL. The analysis of the proposed structure has been performed using the well-known solar cell simulation tool SCAPS-1d. It has been shown that the doping concentration of the two doped sections of the $MaPbI_3$ has an important role to play in deciding the PCE due to the misalignment in the energy band diagram. A doping concentration of 10^{17} cm^{-3} and 10^{16} cm^{-3} on the p and n-doped side, respectively, provides a better band alignment with the ETL and results in high efficiency. Furthermore, the ratio of the p and n-doped sections has been optimized to achieve the maximum PCE, keeping the entire thickness constant at 540 nm. The optimized thickness ratio of the p and n-doped section is found to be 60:40 in %. The presence of graphene in the TiO_2-based ETL layer is found to be helpful in improving the PCE of the proposed structure due to the increment in saturated current density and fill factor. The effect of graphene concentration is more prominent for the higher thickness of the ETL layer. The efficiency is found to be 22.71% for a 100 nm thick gr-TiO_2 nanocomposite layer with a graphene concentration of around 1%.

References

[1] M. Kulbak, D. Cahen, and G. Hodes, "How important is the organic part of lead halide perovskite photovoltaic cells? Efficient CsPbBr3 cells," *J. Phys. Chem. Lett.*, vol. 6, no. 13, pp. 2452–2456, Jun. 2015, doi: 10.1021/acs.jpclett.5b00968.

[2] P. Gao, M. Grätzel, and M. K. Nazeeruddin, "Organohalide lead perovskites for photovoltaic applications," *Energy Environ. Sci.*, vol. 7, no. 8, pp. 2448–2463, Feb. 2014, doi: 10.1021/acs.jpclett.5b02893.

[3] A. Kojima, K. Teshima, Y. Shirai, and T. Miyasaka, "Organometal halide perovskites as visible-light sensitizers for photovoltaic cells," *J. Amer. Chem. Soc.*, vol. 131, no. 17, pp. 6050–6051, Apr. 2009, doi: 10.1021/ja809598r.

[4] R. Verduci et al., "Solar energy in space applications: Review and technology perspectives," *Adv. Energy Mater.*, vol. 12, no. 29, Jun. 2022, Art. no. 2200125, doi: 10.1002/aenm.202200125.

[5] D. Y. Son et al., "Self-formed grain boundary healing layer for highly efficient CH3NH3PbI3 perovskite solar cells," *Nature Energy*, vol. 1, no. 7, pp. 1–8, Jun. 2016, doi: 10.1038/nenergy.2016.81.

[6] D. Wei et al., "A TiO_2 embedded structure for perovskite solar cells with anomalous grain growth and effective electron extraction," *J. Mater. Chem. A*, vol. 5, no. 4, pp. 1406–1414, Dec. 2016, doi: 10.1039/C6TA10418E.

[7] S. Ye et al., "A strategy to simplify the preparation process of perovskite solar cells by co-deposition of a hole-conductor and a perovskite layer," *Adv. Mater.*, vol. 28, no. 43, pp. 9648–9654, Sep. 2016, doi: 10.1002/adma.201603850.

[8] Y. Wu et al., "Perovskite solar cells with 18.21% efficiency and area over 1 cm2 fabricated by heterojunction engineering," *Nature Energy*, no. 1, no. 11, pp. 1–7, Sep. 2016, doi: 10.1038/nenergy.2016.148.

[9] P. Cui et al., "Planar p–n homojunction perovskite solar cells with efficiency exceeding 21.3%," *Nature Energy*, vol. 4, no. 2, pp. 150–159, Feb. 2019, doi: 10.1038/s41560-018-0324-8.

[10] D. K. Maram, M. Haghighi, O. Shekoofa, H. Habibiyan, and H. Ghafoorifard, "A modeling study on utilizing ultra-thin inorganic HTLs in inverted p–n homojunction perovskite solar cells," *Sol. Energy*, vol. 213, pp. 1–12, Jan. 2021, doi: 10.1016/j.solener.2020.11.009.

[11] Q. He, H. Gu, D. Zhang, G. Fang, and H. Tian, "Theoretical analysis of effects of doping MAPbI3 into PN homojunction on several types of perovskite solar cells," *Opt. Mater.*, vol. 121, Nov. 2021, Art. no. 111491, doi: 10.1016/j.optmat.2021.111491.

[12] R. Yousuf and G. Qazi, "Numerical modelling: Design and investigation of uniformly and non-uniformly doped absorber layer based PN homojunction perovskite solar cell variants," *Sol. Energy*, vol. 228, pp. 427–438, Nov. 2021, doi: 10.1016/j.solener.2021.09.079.

[13] Y. Da and M. Xie, "Device physics of homojunction perovskite solar cells: A design omitting all the charge transport layers with efficiency exceeding 26.3%," *J. Phys. D*, vol. 55, no. 28, Apr. 2022, Art. no. 285102, doi: 10.1088/1361-6463/ac5fd3.

[14] D. Khan, S. Sajid, S. Khan, J. Park, and I. Ullah, "Identifying the potentials for charge transport layers free NP homojunction-based perovskite solar cells," *Sol. Energy*, vol. 238, pp. 69–77, May 2022, doi: 10.1016/j.solener.2022.04.034.

[15] M. Acik and S. B. Darling, "Graphene in perovskite solar cells: Device design, characterization and implementation," *J. Mater. Chem. A*, vol. 4, no. 17, pp. 6185–6235, Mar. 2016, doi: 0.1039/C5TA09911K.

[16] S. Pescetelli et al., "Integration of two-dimensional materials-based perovskite solar panels into a stand-alone solar farm," *Nature Energy*, vol. 7, no. 7, pp. 597–607, Apr. 2022, doi: 10.1038/s41560-022-01035-4.

[17] A. Agresti et al., "Graphene–perovskite solar cells exceed 18% efficiency: A stability study," *ChemSusChem*, vol. 9, no. 18, pp. 2609–2619, Sep. 2016, doi: 10.1002/cssc.201600942.

[18] F. Biccari et al., "Graphene-based electron transport layers in perovskite solar cells: A step-up for an efficient carrier collection," *Adv. Energy Mater.*, vol. 7, no. 22, Sep. 2017, Art. no. 1701349, doi: 10.1002/aenm.201701349.

[19] J. T. W. Wang et al., "Low-temperature processed electron collection layers of graphene/TiO2 nanocomposites in thin film perovskite solar cells," *Nano Lett.*, vol. 14, no. 2, pp. 724–730, Dec. 2013, doi: 10.1021/nl403997a.

[20] P. Mariani et al., "Low-temperature graphene-based paste for large-area carbon perovskite solar cells," *Amer. Chem. Soc. Appl. Mater. Interfaces*, vol. 13, no. 19, pp. 22368–22380, May 2021, doi: 0.1021/acsami.1c02626.

[21] R. Belchi et al., "One-step synthesis of TiO2/graphene nanocomposites by laser pyrolysis with well-controlled properties and application in perovskite solar cells," *Amer. Chem. Soc. Omega*, vol. 4, no. 7, pp. 11906–11913, Jul. 2019, doi: 10.1021/acsomega.9b01352.

[22] M. S. Salem et al., "Analysis of hybrid hetero-homo junction lead-free perovskite solar cells by SCAPS simulator," *Energies*, vol. 14, no. 18, Sep. 2021, Art. no. 5741, doi: 10.3390/en14185741.

[23] T. Kirchartz and D. Cahen, "Minimum doping densities for p–n junctions," *Nature Energy*, vol. 5, no. 12, pp. 973–975, Oct. 2020, doi: 10.1038/s41560-020-00708-2.

[24] A. Niemegeers, M. Burgelman, K. Decock, S. Degrave, and J. Verschraegen, "One Dimensional Solar Cell Simulation Program; SCAPS 3.3.10.," [Online]. Available: https://scaps.elis.ugent.be/

[25] I. Alam and M. A. Ashraf, "Effect of different device parameters on tin-based perovskite solar cell coupled with In_2S_3 electron transport layer and CuSCN and Spiro-OMeTAD alternative hole transport layers for high-efficiency performance," *Energy Sources, A, Recovery, Utilization, Environ. Effects*, pp. 1–17, Sep. 2020, doi: 10.1080/15567036.2020.1820628.

[26] M. Dadashbeik, D. Fathi, and M. Eskandari, "Design and simulation of perovskite solar cells based on graphene and TiO2/graphene nanocomposite as electron transport layer," *Sol. Energy*, vol. 207, pp. 917–924, 2020, doi: 10.1016/j.solener.2020.06.102.

[27] S. Karthick, J. Boucl´e, and S. Velumani, "Effect of bismuth iodide (BiI3) interfacial layer with different HTL's in FAPI based perovskite solar cell–SCAPS–1D study," *Sol. Energy*, vol. 218, pp. 157–168, Apr. 2021, doi: 10.1016/j.solener.2021.02.041.

[28] J. M. Ball et al., "Optical properties and limiting photocurrent of thin-film perovskite solar cells," *Energy Environ. Sci.*, vol. 8, no. 2, pp. 602–609, Dec. 2014, doi: 10.1039/C4EE03224A.

[29] S. Mushtaq et al., "Performance optimization of lead-free MASnBr3 based perovskite solar cells by SCAPS-1D device simulation," *Sol. Energy*, vol. 249, pp. 401–413, Jan. 2023, doi: 0.1016/j.solener.2022.11.050.

[30] Y. Da, Y. Xuan, and Q. Li, "Quantifying energy losses in planar perovskite solar cells," *Sol. Energy Mater. Sol. Cells*, vol. 174, pp. 206–213, 2018, doi: 10.1016/j.solmat.2017.09.002.

[31] T. Minemoto and M. Murata, "Theoretical analysis on effect of band offsets in perovskite solar cells," *Sol. Energy Mater. Sol. Cells*, vol. 133, pp. 8–14, Feb. 2015, doi: 10.1016/j.solmat.2014.10.036.

[32] T. Yokoyama et al., "Improving the open-circuit voltage of Sn-based perovskite solar cells by band alignment at the electron transport layer/perovskite layer interface," *Amer. Chem. Soc. Appl. Mater. Interfaces*, vol. 12, no. 24, pp. 27131–27139, May 2020, doi: 10.1021/acsami.0c04676.

Open Access funding provided by 'Politecnico di Bari' within the CRUI CARE Agreement